High Power Laser Science and Engineering, (2024), Vol. 12, e63, 6 pages.
doi:10.1017/hpl.2024.61

HIGH POWER LASER SCIENCE AND ENGINEERING

RESEARCH ARTICLE

Efficient high-power 2.3 μm continuous-wave laser operation of diffusion-bonded composite YVO_4/Tm:$GdVO_4$ crystals

Xiaoxu Yu[1], Zhongben Pan[1], Han Pan[1], Hongwei Chu[1], Weidong Chen[2], and Dechun Li[1]

[1] *School of Information Science and Engineering, Key Laboratory of Laser and Infrared System of Ministry of Education, Shandong University, Qingdao, China*

[2] *Fujian Institute of Research on the Structure of Matter, Chinese Academy of Sciences, Fuzhou, China*

(Received 18 June 2024; revised 2 August 2024; accepted 27 August 2024)

Abstract

We reported on an efficient high-power continuous-wave laser operation on the $^3H_4 \rightarrow {}^3H_5$ transition of Tm^{3+} ions in a diffusion-bonded composite YVO_4/Tm:$GdVO_4$ crystal. Pumped by a laser diode at 794 nm, a maximum output power of 7.5 W was obtained from a YVO_4/Tm:$GdVO_4$ laser at 2.29 μm, corresponding to a slope efficiency of 40.3% and exceeding the Stokes limit. To the best of our knowledge, this result represents the maximum power ever achieved from a Tm laser at 2.3 μm.

Keywords: composite YVO_4/Tm:$GdVO_4$ crystal; high-power Tm laser; $^3H_4 \rightarrow {}^3H_5$ transition

1. Introduction

Short-wave infrared (SWIR) laser sources emitting in the 'molecular fingerprint' spectral range of 2–3 μm are attractive for atmosphere gas sensing, pollutant detection and non-invasive glucose blood measurements[1–3]. Such laser sources are also interesting for pumping of mid-infrared optical parametric oscillators[4]. Tm^{3+} ions (electronic configuration: $[Xe]4f^{12}$) could provide this SWIR emission due to the $^3H_4 \rightarrow {}^3H_5$ 4f-4f transition[5].

However, limited by the large quantum defect (~65%), severe thermal effects and an easily quenched upper laser level ($^3H_4$) lifetime by both the multi-phonon non-radiative (NR) relaxation and cross-relaxation (CR) (see Figure 1), realizing the efficient high-power continuous-wave (CW) laser operation on the $^3H_4 \rightarrow {}^3H_5$ Tm^{3+} transition at 2.3 μm is still a challenge. To date, several Tm^{3+}-doped oxides, that is, aluminates[6–11], vanadates[12–15], tungstate[16] and fluorides[6–18], have been achieved with 2.3 μm laser operation. Pumped by a CW Ti:sapphire laser, 2.3 μm Tm lasers tend to have a high slope efficiency (η) but a relatively low output power (P) due to the limited available pump power, for example, $\eta = 69.2\%$ and $P = 1.12$ W for Tm:$KLu(WO_4)_2$[16], $\eta = 61.8\%$ and $P = 0.96$ W for Tm:$YAlO_3$[7], $\eta = 46.3\%$ and $P = 1.07$ W for Tm:$Y_3Al_5O_{12}$[11], $\eta = 47.3\%$ and $P = 0.73$ W for Tm:$LiYF_4$[17]. Employing commercially available high-power laser diodes as a pump source is expected to realize power scalable at 2.3 μm for Tm lasers. Despite several reports on diode-pumped Tm lasers at 2.3 μm, the slope efficiencies are still limited and do not exceed the Stokes limit[6,8,10,12–14].

Several schemes for power scaling operation of the 2.3 μm Tm lasers have been proposed, for example, up-conversion pumping for Tm:$CaGdAlO_4$ lasers[9] and the cascade lasing strategy for Tm:$YAlO_3$[8], Tm:$CaGdAlO_4$[9], Tm:YVO_4[15] and Tm:$LiYF_4$[18] lasers. Under these schemes, the performance of the Tm laser at 2.3 μm was improved. However, the severe thermal effects remain a key issue, limiting the development of a high-power Tm laser at 2.3 μm. The thermal issues were not effectively alleviated. Recently, a novel intracavity up-conversion pumping scheme has been demonstrated for better and easier thermal management. Under this scheme, a CW Tm:$LiYF_4$ laser delivered 1.81 W at 2.3 μm[19].

The well-developed advances in the manufacturing of diffusion-bonded composite laser crystals give the laser crystals an additional function in that the bonded end cap serves as a heat sink for the pumping surface, thus

Correspondence to: Z. Pan and D. Li, School of Information Science and Engineering, Shandong University, Qingdao 266237, China. Emails: zhongbenpan@sdu.edu.cn (Z. Pan); dechun@sdu.edu.cn (D. Li)

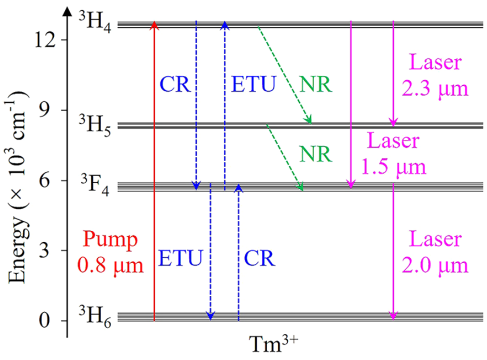

Figure 1. Partial energy-level scheme of Tm^{3+} ions in $GdVO_4$: red and pink arrows, pump and laser transitions, respectively; green arrows, multi-phonon non-radiative (NR) relaxation; blue arrows, cross-relaxation (CR) and energy-transfer up-conversion (ETU) processes.

promoting efficient thermal dissipation and reducing the thermal lensing effect. It has been widely used in Nd^{3+}-doped vanadate crystals, for example, YVO_4/Nd:$GdVO_4$[20], YVO_4/Nd:YVO_4/YVO_4[21] and $LuVO_4$/Nd:$LuVO_4$/$LuVO_4$[22], as well as other RE^{3+}-doped laser crystals, for example, YSGG/Er:YSGG/YSGG[23], YAG/Tm:YAG[24] and Yb^{3+}:$SrY_4(SiO_4)_3O$||$Y_2Al_5O_{12}$[25]. To the best of our knowledge, there are no reports with respect to improving the output performance of 2.3 μm Tm lasers by bonded composite laser crystals.

In recent years, the Tm^{3+}-doped rare-earth orthovanadate $REVO_4$ (RE = Gd, Y or Lu) has attracted a great deal of attention due to the relatively good thermo-mechanical properties of the host matrices and the broad and smooth absorption and emission spectral bands of the Tm^{3+} ions. In particular, Tm^{3+}-doped $GdVO_4$ crystals offer a higher thermal conductivity (9.9 W/(m·K) for undoped *a*-cut $GdVO_4$[26]), a lower thermal expansion (1.19×10^{-6} K^{-1} for the *a*-axis[27]) and a relatively high thermal shock parameter[26], making them more suitable for use as the gain media of high-power lasers. Very recently, an approximately 6 W level CW laser operating on the $^3H_4 \rightarrow {}^3H_5$ Tm^{3+} transition was obtained with a 1.5% (atomic fraction) *a*-cut Tm:$GdVO_4$ crystal[12], which was the highest CW laser power amongst the reported 2.3 μm Tm lasers. However, its laser slope efficiency (30.8%, below the Stokes limit of ~34.5%) is relatively low. The relatively good 2.3 μm laser performance of the Tm:$GdVO_4$ crystal motivates us to further study the power scaling operation with diffusion-bonded crystals.

In the present work, we report on a 7.5 W CW YVO_4/Tm:$GdVO_4$ laser operating on the $^3H_4 \rightarrow {}^3H_5$ transition at 2.3 μm. Benefiting from the alleviated thermal effect and the efficient energy-transfer up-conversion (ETU) process at the high pump level, the maximum slope efficiency reached as high as 40.3%, which exceeds the Stokes limit (~34.5%).

2. Simulation

The temperature field distributions in YVO_4/Tm:$GdVO_4$ and Tm:$GdVO_4$ crystals were simulated by the finite element method. In the simulation, the pump spot diameter at the incident end face of the gain media was set to 200 μm. The power and wavelength of the pump beam were set to 23 W and 794 nm, respectively. The Tm^{3+} doping level used for simulation was 1.5% (atomic fraction), corresponding to the actual Tm^{3+} ion densities of 1.82×10^{20} cm^{-3}. The absorption coefficient (α) was calculated to be 1.44 cm^{-1}. The coordinate system used in the simulation is shown in Figure 2(a). The dimensions of the crystals used for simulation are 3 mm × 3 mm × 10 mm. For the composite crystals, the dimensions of the bonded undoped end cap (YVO_4) and the Tm^{3+}-doped $GdVO_4$ were 3 mm × 3 mm × 3 mm and 3 mm × 3 mm × 7 mm, respectively. The pump beam is incident along the –*Z*-axis into the laser crystals. The highest temperature appears at the center of the incident end face ($X = Y = 1.5$ mm, $Z = 10$ mm) for the Tm:$GdVO_4$ crystal and below the bonding surface ($X = Y = 1.5$ mm, $Z = 7$ mm) for the YVO_4/Tm:$GdVO_4$ crystal, as shown in Figures 2(b) and 2(c), respectively. Compared with the Tm:$GdVO_4$ crystal, the thermal lensing

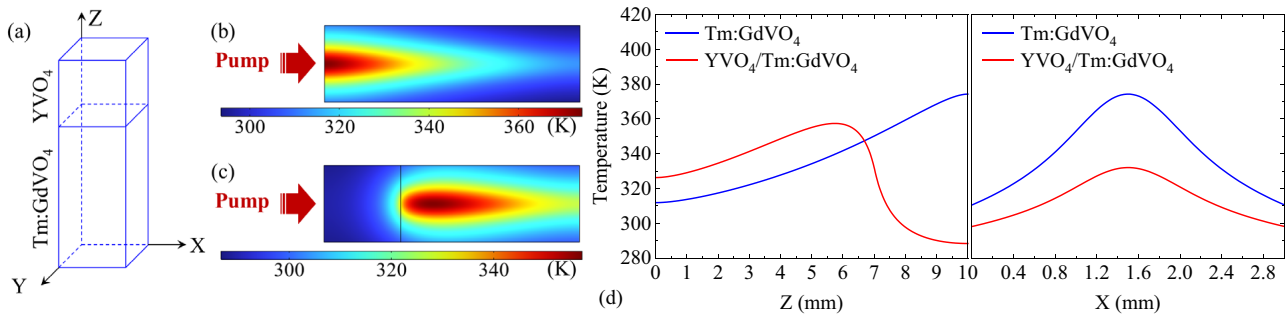

Figure 2. (a) Coordinate system used in the simulation. Cross-section view ($X = 1.5$ mm) of the temperature field distribution in diode end pumped (b) Tm:$GdVO_4$ and (c) YVO_4/Tm:$GdVO_4$ crystals. (d) Temperature field distribution on the axis of the cross-section ($X = 1.5$ mm) and the incident end face of the gain media.

https://doi.org/10.1017/hpl.2024.61 Published online by Cambridge University Press

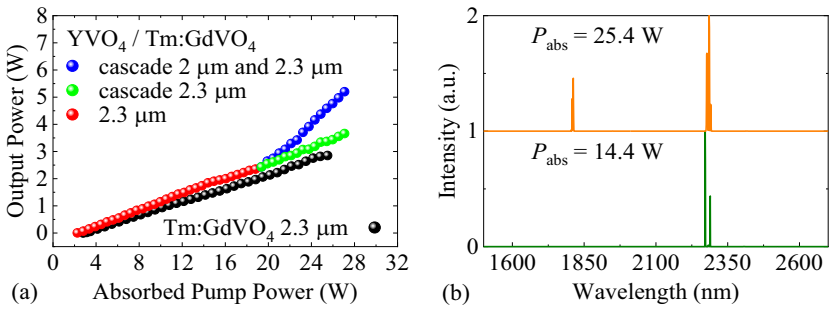

Figure 3. (a) Input–output dependences and (b) typical laser emission spectra of the diode-pumped Tm:$GdVO_4$ and YVO_4/Tm:$GdVO_4$ lasers operating on the $^3H_4 \rightarrow {}^3H_5$ transition: 2% OC, using the same laser cavity parameters as in our previous work[12].

effect can be effectively alleviated in the composite YVO_4/Tm:$GdVO_4$ crystal due to the drastically reduced temperature (from 374 to 288 K) at the incident end face. Furthermore, it has a more uniform longitudinal temperature distribution.

The temperature field distributions are compared in detail in Figure 2(d). On the axis of the cross-section ($X = 1.5$ mm), the maximum temperatures were 374 and 357 K, for the Tm:$GdVO_4$ and YVO_4/Tm:$GdVO_4$ crystals, respectively. On the axis of the incident end face of the gain media, they were 374 and 332 K, respectively. Compared with the Tm:$GdVO_4$ crystal, there was a lower maximum temperature and temperature difference in the composite crystals.

3. Experimental results and discussion

The undoped YVO_4 and Tm^{3+}-doped $GdVO_4$ crystals (Tm^{3+} doping level, 1.5% atomic fraction) were grown by the conventional Czochralski method. The composite YVO_4/Tm:$GdVO_4$ crystal was further fabricated by the diffusion bonding method. The Tm:$GdVO_4$ and YVO_4/Tm:$GdVO_4$ crystals with the same dimensions as those used in the simulation were employed as the gain media. They were oriented for light propagation along the *a*-axis (*a*-cut). For the Tm:$GdVO_4$ crystal, both the input and output faces were coated for antireflection (AR) at 790 ± 10 nm (reflectance (R) < 0.5%) and 1850–2360 nm (R < 1%). The composite YVO_4/Tm:$GdVO_4$ crystal was uncoated. A fiber-coupled spatially multimode AlGaAs laser diode (fiber core diameter, 200 μm; numerical aperture (NA), 0.22) with a central emission wavelength of 794 nm was used as the pump source. The pump beam was reimaged into the laser crystal by a pair of plano-convex lenses (focal length, $f = 50$ mm), providing a pump spot radius of about 100 μm.

The pump absorption efficiency of the YVO_4/Tm:$GdVO_4$ crystal under non-lasing conditions was measured in a pump-transmission experiment. It ranges from 63.0% to 53.6% on increasing the pump level after considering the reflection loss. Note that in this work, all the laser slope efficiencies are fitted versus absorbed pump power and all the laser thresholds refer to the absorbed pump power.

Firstly, we tested the laser performance of the YVO_4/Tm:$GdVO_4$ crystal using the same laser cavity parameters as in our previous work[12]. However, at the high pump level, co-lasing cannot be avoided, that is, the YVO_4/Tm:$GdVO_4$ lasers operated on the cascade state (simultaneously operating on the $^3H_4 \rightarrow {}^3H_5$ and $^3F_4 \rightarrow {}^3H_6$ transitions). We believe this may originate from the reduced gain and the increased loss, which leads to the $^3F_4 \rightarrow {}^3H_6$ transition dominating the gain competition between it and the $^3H_4 \rightarrow {}^3H_5$ one. The cascade lasing threshold decreased with the increase in transmission of the output coupler (OC). Figure 3 shows the input–output dependences and the typical laser emission spectra of the YVO_4/Tm:$GdVO_4$ laser with a 2% OC. The maximum CW output power reached 3.66 W at 2.29 μm with a slope efficiency of 15.5% and a laser threshold of 2.27 W. Although the laser performance has not been significantly improved, it was relatively good compared to the use of unbonded Tm:$GdVO_4$ crystals reported in our previous work[12], that is, 2.85 W at 2.29 and 2.36 μm with a lower laser slope efficiency of 12.6% and a laser threshold of 2.8 W.

A schematic of the modified laser cavity is depicted in Figure 4. The 3.7-cm long linear plano-concave cavity consisted of a concave pump mirror (PM; the radius of curvature (R_{PM}), 50 mm) coated for AR at 770–820 nm and 1800–2100 nm (reflectance (R) < 0.2%) and high reflection at 2250–2500 nm (R > 99.6%) and a set of flat OCs providing a transmission T_{OC} ranging from 0.5% to 10% at

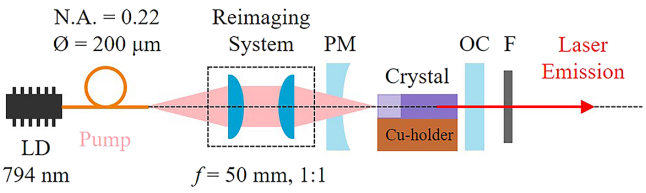

Figure 4. Schematic of the diode-pumped Tm:$GdVO_4$ or YVO_4/Tm:$GdVO_4$ laser. LD, laser diode; PM, pump mirror; OC, output coupler; F, long-wavelength-pass filter.

https://doi.org/10.1017/hpl.2024.61 Published online by Cambridge University Press

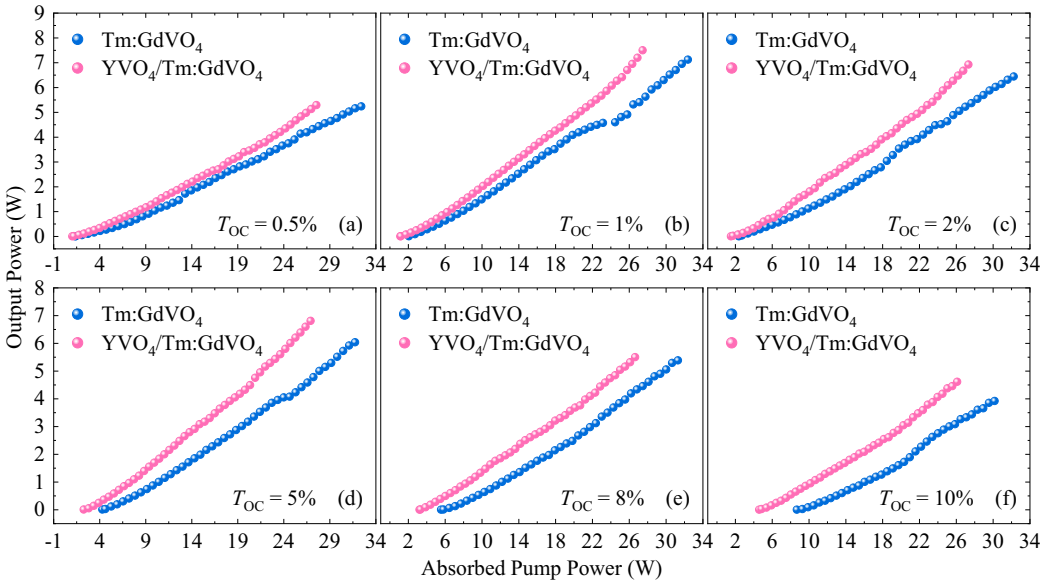

Figure 5. Input–output dependences of the diode-pumped Tm:$GdVO_4$ and YVO_4/Tm:$GdVO_4$ lasers operating on the $^3H_4 \rightarrow {}^3H_5$ transition: (a)–(f) 0.5%–10% OCs.

2.2–2.4 μm. All the OCs additionally provided a high transmission of approximately 90% at around 2 μm. The laser crystal was wrapped with indium foil and mounted inside a water-cooled copper block with the temperature set at 12°C.

The input–output dependences of the diode-pumped 2.3 μm Tm:$GdVO_4$ and YVO_4/Tm:$GdVO_4$ lasers are shown in Figure 5. For all the studied OCs, these two lasers operated solely on the $^3H_4 \rightarrow {}^3H_5$ Tm^{3+} transition without co-lasing at 2 μm. Noting that all the power transfer curves were nonlinear, the laser slope efficiencies were fitted at lower and higher pump levels, respectively, in this work.

For the unbonded Tm:$GdVO_4$ laser, the maximum CW laser output power of 7.12 W was obtained by the 1% OC with a slope efficiency of 32.4%. Another higher power of 6.44 W was obtained by the 2% OC. Compared with the laser cavity used in our previous work[12], this laser cavity provided a higher laser slope efficiency due to the relatively good mode-matching.

Compared with the Tm:$GdVO_4$ laser, the YVO_4/Tm:$GdVO_4$ one possessed better laser performance, for example, a lower laser threshold, higher slope efficiency and higher output power, due to the alleviated thermal effects. Its highest CW laser output power reached 7.5 W with a lower laser threshold of only 1.13 W at 2.29 μm for the 1% OC at the incident pump power of 45 W. The optical-to-optical efficiency was about 17%. The corresponding laser slope efficiency increased gradually from 25.6% to 40.3% as the pump level increased. At the maximum incident pump power, no thermal roll-over or crystal thermal fracture was observed, and the bonding surface between the YVO_4 and Tm:$GdVO_4$ was not damaged. Further power scaling was limited only by the available pump power. Furthermore, a better laser performance was expected by coating for AR at the pump and laser wavelengths on both the end faces of the YVO_4/Tm:$GdVO_4$ crystal. To the best of our knowledge, both the 2.3 μm CW laser power (7.5 W) and the laser slope efficiency (40.3%, exceeding the Stokes limit, $\eta_{St,L} = \lambda_P / \lambda_L = 34.5\%$) far surpass the best results of reported diode-pumped Tm lasers operating on the $^3H_4 \rightarrow {}^3H_5$ transition, as shown in Table 1. For higher output coupling of 2% and 5%, the laser performance was also relatively excellent. The maximum CW laser output powers could also reach an approximately 7 W level with a slope efficiency exceeding or close to the Stokes limit ($P = 6.93$ W, $\eta = 35.9\%$ for the 2% OC and $P = 6.81$ W, $\eta = 33.9\%$ for the 5% OC). Noting that there was a similar behavior of the gradual increase in the slope efficiency for all the OCs, we believe that it is mainly due to the positive action of the ETU effect, which was responsible for refilling the upper laser level ($^3H_4$) at the expense of the $^3F_4$ population. Under this condition, the pump quantum efficiency of the $^3H_4 \rightarrow {}^3H_5$ transition increased and may exceed unity, leading to the laser slope efficiency exceeding the Stokes limit[17]. Note that the laser thresholds of the non-bonded crystal are almost twice as high compared to the bonded crystal. We believe this was mainly caused by the severe thermal effects due to higher temperatures. Differences in the quality of the two crystals and the possible experimental errors also contributed. More details not mentioned in the above text can be found in Table 1.

The typical laser emission spectra of the YVO_4/Tm:$GdVO_4$ laser with 0.5%–10% OCs captured at the maximum output power are shown in Figure 6(a). Using an output coupling of 0.5%, this laser operated in two spectral ranges, at 2.37 and 2.29 μm, corresponding to the two emission peaks of the $^3H_4 \rightarrow {}^3H_5$ Tm^{3+} transition (π-polarization)[12]. Using an OC with higher output coupling transmittance, that

https://doi.org/10.1017/hpl.2024.61 Published online by Cambridge University Press

Table 1. Performance comparison of the diode-pumped Tm:$GdVO_4$, YVO_4/Tm:$GdVO_4$ and other reported CW Tm lasers operating on the $^3H_4 \rightarrow {}^3H_5$ transition[a].

Crystal	T_{OC} (%)	P_{th} (W)	P_{max} (W)	η (%)	Ref.
Tm:$GdVO_4$	0.5	1.34	5.24	9.40–18.9	This work
	1	2.06	7.12	17.0–32.4	
	2	2.38	6.44	15.0–25.0	
	5	4.28	6.04	18.0–28.4	
	8	5.56	5.39	16.1–25.1	
	10	8.67	3.92	15.4–20.6	
YVO_4/Tm:$GdVO_4$	0.5	1.02	5.29	15.7–25.4	This work
	1	1.13	7.50	25.6–40.3	
	2	1.52	6.93	17.8–35.9	
	5	2.26	6.81	23.9–33.9	
	8	3.21	5.50	20.0–28.5	
	10	4.58	4.61	17.1–27.3	
Tm:YVO_4	1	2.99	1.89	13.6	[13]
Tm:$GdVO_4$	5	4.80	6.09	30.8	[12]
Tm:$LuVO_4$	5	8.51	0.99	9.20	[14]
Tm:$YAlO_3$	2	6.24	2.97	21.4	[8]
Tm:$Y_3Al_5O_{12}$	1	3.80	1.49	10.1	[10]
Tm:$LiYF_4$	0.7	0.72	2.11[b]	26.9	[6]
	2.5	10.0	1.81	5.70[c]	[19]

[a]T_{OC}, transmission of the OCs at 2.3 μm; P_{th}, laser threshold power (absorbed pump power); P_{max}, maximum CW laser output power; η, laser slope efficiency (versus absorbed pump power); Ref., reference.
[b]Quasi-CW laser power.
[c]Laser slope efficiency versus incident pump power.

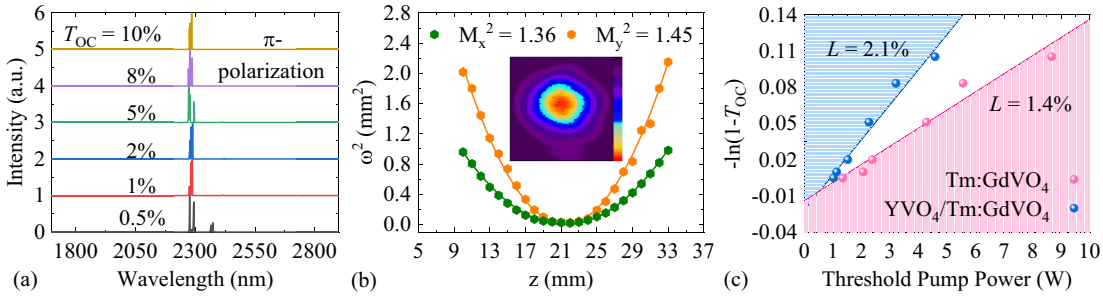

Figure 6. (a) Typical laser emission spectra of the YVO_4/Tm:$GdVO_4$ laser at the maximum output level. (b) Measured beam quality (M^2) with the 1% OC, inset: two-dimensional laser beam profile. (c) Findlay–Clay analysis for Tm:$GdVO_4$ and YVO_4/Tm:$GdVO_4$ lasers. L, round-trip intracavity losses.

is, 1%–10%, this laser was simply operated at 2.29 μm. Figure 6(b) shows the evaluation of the beam quality parameters M^2 and laser beam profile (inset) with the 1% OC. The diode-pumped YVO_4/Tm:$GdVO_4$ laser operated close to the fundamental transverse mode and generated a nearly circular output beam. The slight beam ellipticity was probably due to the thermal lens-induced astigmatism. The measured M_x^2 and M_y^2 values were 1.36 and 1.45, respectively. Using the Findlay–Clay analysis[28], the round-trip resonator losses for the Tm:$GdVO_4$ and YVO_4/Tm:$GdVO_4$ lasers were estimated to be 1.4% and 2.1%, respectively, as shown in Figure 6(c). The higher loss for the latter case may be caused by the stronger reflections due to the absence of AR coating at the pump and laser wavelengths on both the end faces of the YVO_4/Tm:$GdVO_4$ crystal. Therefore, a further decrease in the laser threshold and an increase in the slope efficiency are expected, thus leading to a higher 2.3 μm CW laser output power.

4. Conclusion

To conclude, the power scaling operation of a 2.3 μm Tm laser with a diffusion-bonded composite YVO_4/Tm:$GdVO_4$ crystal was studied for the first time. This laser delivered a maximum CW laser output power of 7.5 W with a slope efficiency as high as 40.3%, exceeding the Stokes limit. Both the power and efficiency are the highest ever achieved from any diode-pumped Tm laser operating on the $^3H_4 \rightarrow {}^3H_5$ transition, demonstrating the great potential of the YVO_4/Tm:$GdVO_4$ crystal for diode-pumped efficient high-power 2.3 μm Tm lasers. This composite crystal is of extremely high quality and was not damaged during the experiment. By employing a laser diode capable of delivering higher pump power as the pump source and (or) coating for AR at the pump and laser wavelengths on both the end faces of the YVO_4/Tm:$GdVO_4$ crystal to reduce the loss, etc., further power scaling operation is expected.

https://doi.org/10.1017/hpl.2024.61 Published online by Cambridge University Press

Acknowledgements

This work was supported by the National Natural Science Foundation of China (Nos. 52072351, 12274263, 12174223 and 12304466), the Qilu Young Scholar Program of Shandong University and the Taishan Scholar Foundation of Shandong Province.

References

1. X. Chao, J. B. Jeffries, and R. K. Hanson, Appl. Phys. B **110**, 359 (2013).
2. M. E. Webber, J. Wang, S. T. Sanders, D. S. Baer, and R. K. Hanson, Proc. Combust. Inst. **28**, 407 (2000).
3. S. T. Fard, W. Hofmann, P. T. Fard, G. Böhm, M. Ortsiefer, E. Kwok, M. C. Amann, and L. Chrostowski, IEEE Photonics Technol. Lett. **20**, 930 (2008).
4. V. Petrov, Prog. Quantum Electron. **42**, 1 (2015).
5. J. A. Caird, L. G. Deshazer, and J. Nella, IEEE J. Quantum Electron. **11**, 874 (1975).
6. E. Kifle, P. Loiko, L. Guillemot, J.-L. Doualan, F. Starecki, A. Braud, T. Georges, J. Rouvillain, and P. Camy, Appl. Opt. **59**, 7530 (2020).
7. L. Guillemot, P. Loiko, E. Kifle, A. Braud, J.-L. Doualan, A. Hideur, M. Koselja, R. Moncorgé, and P. Camy, Proc. SPIE **11357**, 113570H (2020).
8. X. Yu, F. Zha, Z. Pan, H. Chu, H. Pan, and D. Li, Opt. Express **32**, 3461 (2024).
9. H. Dupont, P. Loiko, A. Tyazhev, L. Giordano, Z. Pan, H. Chu, D. Li, B. Viana, A. Hideur, L. Guillemot, A. Braud, P. Camy, P. Georges, and F. Druon, Opt. Express **31**, 18751 (2023).
10. F. Zha, X. Yu, H. Chu, H. Pan, S. Zhao, P. Loiko, Z. Pan, and D. Li, Opt. Lett. **47**, 6265 (2022).
11. L. Guillemot, P. Loiko, E. Kifle, J.-L. Doualan, A. Braud, F. Starecki, T. Georges, J. Rouvillain, A. Hideur, and P. Camy, Opt. Mater. **101**, 109745 (2020).
12. X. Yu, K. Eremeev, Z. Pan, P. Loiko, H. Chu, H. Pan, S. Zhao, A. Braud, P. Camy, and D. Li, Opt. Lett. **48**, 6404 (2023).
13. X. Yu, H. Chu, F. Zha, H. Pan, S. Zhao, Z. Pan, and D. Li, Opt. Lett. **47**, 5501 (2022).
14. X. Yu, K. Eremeev, Z. Pan, P. Loiko, H. Chu, H. Pan, A. Braud, P. Camy, and D. Li, Opt. Express **32**, 19611 (2024).
15. X. Yu, K. Eremeev, Z. Pan, P. Loiko, H. Chu, H. Pan, A. Braud, P. Camy, and D. Li, Opt. Express **32**, 18055 (2024).
16. P. Loiko, E. Kifle, L. Guillemot, J.-L. Doualan, F. Starecki, A. Braud, M. Aguiló, F. Díaz, V. Petrov, X. Mateos, and P. Camy, J. Opt. Soc. Am. B. **38**, 482 (2021).
17. P. Loiko, R. Soulard, L. Guillemot, G. Brasse, J.-L. Doualan, A. Braud, A. Tyazhev, A. Hideur, F. Druon, and P. Camy, IEEE J. Quantum Electron. **55**, 1700212 (2019).
18. H. Dupont, L. Guillemot, P. Loiko, R. M. Solé, X. Mateos, M. Aguiló, F. Díaz, A. Braud, P. Camy, P. Georges, and F. Druon, Opt. Express **31**, 34201 (2023).
19. H. Dupont, T. Lenfant, L. Guillemot, P. Loiko, X. Delen, P. Loiseau, B. Viana, T. Georges, P. Georges, P. Camy, and F. Druon, Opt. Lett. **49**, 2093 (2024).
20. D. Chen, X. Li, Y. Zhang, X. Yu, F. Chen, R. Yan, Y. Ma, and C. Wang, Laser Phys. Lett. **8**, 46 (2011).
21. X. Chen, X. Zhang, Q. Wang, P. Li, Z. Liu, Z. Cong, L. Li, and H. Zhang, Appl. Phys. B **106**, 653 (2012).
22. Y. Lü, X. Zhang, S. Li, J. Xia, W. Cheng, and Z. Xiong, Opt. Lett. **35**, 2964 (2010).
23. L. Hu, D. Sun, H. Zhang, J. Luo, C. Quan, Z. Han, K. Dong, Y. Chen, and M. Cheng, Infrared Phys. Technol. **119**, 103944 (2021).
24. S. Dai, J. Huang, H. Huang, L. Wu, J. Li, J. Deng, Y. Ge, and W. Lin, Chin. Phys. B **26**, 074211 (2017).
25. F. Druon, S. Chénais, F. Balembois, P. Georges, R. Gaumé, and B. Viana, Opt. Lett. **30**, 857 (2005).
26. J. Petit, P. Loiseau, P. Goldner, B. Viana, D. Vivien, and B. Ferrand, Proc. SPIE **5460**, 132 (2004).
27. P. A. Loiko, K. V. Yumashev, V. N. Matrosov, and N. V. Kuleshov, Appl. Opt. **54**, 4820 (2015).
28. J. A. Caird, S. A. Payne, P. R. Staver, A. J. Ramponi, L. L. Chase, and W. F. Krupke, IEEE J. Quantum Electron. **24**, 1077 (1988).

https://doi.org/10.1017/hpl.2024.61 Published online by Cambridge University Press